

# Proximity Ligation Assay for High-content Profiling of Cell Signaling Pathways on a Microfluidic Chip\*

Matthias Blazek<sup>‡§¶</sup>, Charles Betz<sup>||</sup>, Michael Nip Hall<sup>||</sup>, Michael Reth<sup>¶\*\*‡‡</sup>, Roland Zengerle<sup>§¶</sup>, and Matthias Meier<sup>¶¶§§</sup>

Here, we present the full integration of a proximity ligation assay (PLA) on a microfluidic chip for systematic cell signaling studies. PLA is an *in situ* technology for the detection of protein interaction, post-translational modification, concentration, and cellular location with single-molecule resolution. Analytical performance advances on chip are achieved, including full automation of the biochemical PLA steps, target multiplexing, and reduction of antibody consumption by 2 orders of magnitude relative to standard procedures. In combination with a microfluidic cell-culturing platform, this technology allows one to gain control over 128 cell culture microenvironments. We demonstrate the use of the combined cell culture and protein analytic assay on chip by characterizing the Akt signaling pathway upon PDGF stimulation. Signal transduction is detected by monitoring the phosphorylation states of Akt, GSK-3 $\beta$ , p70S6K, S6, Erk1/2, and mTOR and the cellular location of FoxO3a in parallel with the PLA. Single-cell PLA results revealed for Akt and direct targets of Akt a maximum activation time of 4 to 8 min upon PDGF stimulation. Activation times for phosphorylation events downward in the Akt signaling pathway including the phosphorylation of S6, p70S6K, and mTOR are delayed by 8 to 10 min or exhibit a response time of at least 1 h. Quantitative confirmation of the Akt phosphorylation signal was determined with the help of a mouse embryonic fibroblast cell line deficient for rictor. In sum, this work with a miniaturized PLA chip establishes a biotechnolog-

ical tool for general cell signaling studies and their dynamics relevant for a broad range of biological inquiry. *Molecular & Cellular Proteomics* 12: 10.1074/mcp.M113.032821, 3898–3907, 2013.

Signal transduction from the extracellular microenvironment to the inner compartments of cells involves the interaction, post-translational modification, and translocation of proteins. Several molecular biology technologies (1–4) have been developed for the quantitative analysis of proteins and their modifications in order to reveal signal dynamics, cross-activations of protein signaling networks, or statistical variations of signals between cells. Predominant are Western blot, time-lapsed fluorescence microscopy, and immunofluorescence assay technologies. For large-scale approaches, however, the standard assays are hampered, although for different reasons. Western blots average millions of cells per data point and provide limited quantitative information. For fluorescence microscopy, long bioengineering processes are required in order to introduce protein labels for each target in a cellular context. In the case of immunofluorescence, the same analytical workflow for the detection of different targets exists (5), but because of the loss of cell integrity during the sample preparation, only one time point per sample can be obtained.

The limitation of low sampling rates also holds true for the proximity ligation assay (PLA).<sup>1</sup> The PLA technology is a versatile immuno-based *in situ* detection system for protein interactions, modifications, concentrations, and cellular location (6). The simplest PLA setup for measuring protein concentrations or modifications requires a primary antibody (Ab) that binds its specific target within a fixed cell. A pair of polyclonal secondary Abs conjugated to different oligonucleotide strands is then used to detect the target bound to the primary Ab. In cases where two differently labeled secondary

From the <sup>‡</sup>Microfluidic and Biological Engineering, IMTEK - Department of Microsystems Engineering, University of Freiburg, Georges-Koehler-Allee 103, 79110 Freiburg, Germany; <sup>§</sup>Laboratory for MEMS Applications, IMTEK - Department of Microsystems Engineering, University of Freiburg, Georges-Koehler-Allee 103, 79110 Freiburg, Germany; <sup>¶</sup>BIOSS - Centre for Biological Signalling Studies, University of Freiburg, 79108 Freiburg, Germany; <sup>||</sup>Biozentrum, University of Basel, CH 4056, Basel, Switzerland; <sup>\*\*</sup>Max Planck Institute of Immunobiology and Epigenetics, D-79108 Freiburg, Germany; <sup>‡‡</sup>Biology III, Faculty of Biology, University of Freiburg, 79108 Freiburg, Germany

Received July 25, 2013, and in revised form, September 25, 2013  
Published, MCP Papers in Press, September 26, 2013, DOI 10.1074/mcp.M113.032821

Author contributions: M.B., M.N.H., M.R., R.Z., and M.M. designed research. M.B. performed research. C.B. and M.N.H. contributed new reagents. M.B. and M.M. analyzed data. M.B. and M.M. wrote the paper.

<sup>1</sup> The abbreviations used are: Ab, antibody; iRicKO, rictor inducible deficient mouse embryonic fibroblast cell line; MEF, mouse embryonic fibroblast; mTORC, mTOR complex; PDGF, platelet-derived growth factor; PDMS, polydimethylsiloxane; PIP3, phosphatidylinositol(3,4,5)-trisphosphate; PLA, proximity ligation assay.

Abs are in close proximity, the oligonucleotide sequences can be complemented, ligated, and amplified by means of rolling circle amplification. Detection of the amplified DNA is achieved through hybridization of a complementary fluorescence probe to the amplified DNA sequence. Positive single PLA events result in a localized DNA polymer with a hydrodynamic diameter of less than 1  $\mu\text{m}$ , which can be detected with low numerical aperture optics (6–8). Similar workflows with two primary Abs exist for the detection of protein interactions (7).

Inherent to all currently applied protein assays for cell signaling studies are low integration levels. Workflows for cell cultivation, stimulation, and protein analytics are separated from one another, which leads to low temporal and chemical control over cell samples with the consequence of low comparability between repeats or experimental time series.

Integrated microfluidic chip technologies can overcome the limitations encountered in large-scale protein analytics. Microfluidics is the science of fluids and their control in micrometer-sized structures (9). Through miniaturization, complex biological workflows can be automated and multiplexed. The advances of microfluidics for cell signaling have been focused mainly on spatial and temporal control over cell microenvironments (10). Chip platforms combining time-lapsed microscopy with automated cell culturing or with fully integrated workflows of immunofluorescence assays (11) are the first steps toward complete analysis systems. But the miniaturization of standard protein assays can also lead to greater precision and throughput, as was shown for Western blots performed in micrometer capillaries (12) and immunoprecipitation assays in microchambers (13).

Here, we demonstrate the full implementation of the proximity ligation assay on a microfluidic chip for profiling high-content information of cell signaling pathways. The microfluidic chip is made of multilayered polydimethylsiloxane (PDMS) and combines a perfusion system for cell culturing and stimulation with a multiplexed PLA. About 540 microfluidic PDMS membrane valves operated by 24 electrical solenoid valves were programmed to control the pressure-driven flow of 24 different fluids through the microchannels and chambers of the chip. Cell chambers were arranged in a two-dimensional matrix design in which each axis of the matrix allowed the sampling of a different assay parameter. A cell chamber is able to hold about 100 fibroblast cells. Precise temporal changes of fluids along each column element were used to vary the stimulation times of fibroblast cells with platelet-derived growth factor (PDGF) in a time frame of minutes to hours. Fixation of the cell cultures with paraformaldehyde at different time points after stimulation maintained the signaling state of the cell on chip and made it accessible for subsequent analysis with the PLA. Multiplexing of the PLA along row elements of the matrix design with primary Abs allowed the measurement of systematic and quantitative signal dynamics of six different phosphorylation sites and one

protein translocation event in the Akt pathway in response to PDGF stimulation. In the following section, we first describe the functionalities of the microfluidic chip platform and then demonstrate its use for general signaling research.

#### EXPERIMENTAL PROCEDURES

**PDMS Chip Fabrication**—The microfluidic devices were fabricated using standard multilayer soft lithography methods (36). In short, SU-8 3025 (MicroChem, Newton, MA) and AZ 40 XT (MicroChemicals, Ulm, Germany) photoresists were used to produce control and flow molds, respectively. The features on the molds were 20  $\mu\text{m}$  in height, with the exception of the cell cultivation chambers, which were 40  $\mu\text{m}$ . For rapid prototyping of the microfluidic chip, we used PDMS (Sylgard 184, Dow Corning, Midland, MI) and bonded the two layers in pushdown valve orientation in an off-ratio procedure. Assembled PDMS chips were plasma bonded to a glass carrier (Brain Laboratories, Newton, MA).

**Device Operation**—The PDMS chips were mounted inside an on-stage cell incubator. Temperature and  $\text{CO}_2$  concentration in the stage incubator were adapted to the corresponding assay step (see below). Control layer ports were connected to solenoid valves (CMC Microsystems, Kingston, Canada), which were controlled by a processing computer. Reagents for cell cultivation, stimulation, and the PLA were filled in either pressurized small-volume glass containers or Tygon tubing (Saint-Gobain, Koeln, Germany) or were connected to the corresponding flow layer inlets. Typical control and flow pressure values during an experiment were 200 and 10 to 30 kPa, respectively.

**Cell Culture and Starvation**—NIH3T3 (DMSZ, Heidelberg, Germany) and mouse embryonic fibroblast (MEF) cells (obtained from M. Hall) were cultured and harvested following standard protocols (ATCC, VA). For on-chip cultivation, the cells were trypsinized, centrifuged, and resuspended in full medium (*i.e.* high-glucose Dulbecco's modified Eagle's medium (DMEM) supplemented with 10% fetal bovine serum (FBS) and 1% PenStrep (all from Invitrogen)) at a concentration of  $\sim 5 \times 10^6$  cells/ml. Before the introduction of the cell suspension onto the chip, cell chambers were coated with 0.05% fibronectin from human plasma (Sigma) for 2 h. Cells were cultured again on chip in full medium for 12 to 24 h at 37 °C and 5%  $\text{CO}_2$ . The cell medium was exchanged every 90 min automatically at a flow rate of 1  $\mu\text{l}/\text{min}$  ( $\sim 7$  kPa). NIH3T3 and MEF cell lines were starved with 0.1% FBS for 14 and 4 h before the stimulation experiments, respectively. The knockdown of rictor in an MEF deficient cell line was induced on chip with tamoxifen (Sigma) for 72 h (34).

**Cell Stimulation, Fixation, and Permeabilization**—For cell stimulation, PDGF-BB (Prospec Technogene, Ness-Ziona, Israel) was diluted to a concentration of 100 ng/ml in high-glucose DMEM. Within a control experiment, cells were first exposed to the PI3K inhibitor LY294002 (Cell Signaling Technology, Denver, MA) for 30 min before PDGF-BB stimulation. LY294002 was diluted to a final concentration of 100  $\mu\text{mol}$  in high-glucose DMEM without FBS. Cells were fixed with 4% formaldehyde (Thermo Fisher Scientific) for 16 min after the indicated stimulation times and permeabilized with 0.05% Tween 20 (Sigma) for 3 min. Permeabilization was performed at room temperature, and all preceding steps were performed at 37 °C under 5%  $\text{CO}_2$ .

**Primary Antibodies**—Prior primary Ab perfusion all channels and cells were blocked with 1 mg/ml BSA dissolved in PBS for 1 h. Monoclonal antibodies (Cell Signaling Technology) were diluted in PBS with 1 mg/ml BSA. In detail, Akt (pan) (No. 4691), Akt (Ser-473) (No. 4060), Akt (Thr-308) (No. 2965), GSK-3 $\beta$  (Ser-9) (No. 9323), p70S6 kinase (Thr-389) (No. 9234), mTOR (Ser-2448) (No. 5536), Erk1/2 (Thr202/Tyr204) (No. 4370), and FoxO3a (No. 2497) were diluted 1:50 unless otherwise indicated. S6 ribosomal protein (Ser-

240/244) (No. 5364) was diluted 1:200. The antibody dilutions were incubated for 14 h at room temperature and exchanged at intervals of 2 h.

**Proximity Ligation Assay**—Oligonucleotide labeled secondary Abs (anti-rabbit Plus and Minus, Olink, Uppsala, Sweden) were incubated for 2 h at room temperature. DNA labels of the secondary Ab were complemented and ligated with a DNA connector (Olink) and T4 ligase (Fermentas, St. Leon-Rot, Germany) for 60 min at 32 °C. The subsequent amplification of the DNA strands was performed at 32 °C with a phi29 polymerase (Fermentas) for 2 h. Finally, the cytoskeleton and nuclei were counterstained with Phalloidin-Atto 488 (Sigma) and 4',6-diamidino-2-phenylindole dihydrochloride (Sigma). After each process step, wash cycles with buffer solutions were introduced.

**Image Acquisition and Analysis**—Image acquisition was done using an Axio Observer inverted fluorescence microscope with a 20× objective and AxioCam MRm and Axio Vision microscope software (Zeiss, Jena, Germany). For each cell culture chamber on the chip, three images were acquired using the filter sets 21HE, 38HE, and 43HE from Zeiss, which correspond to the nuclei, cytoskeleton, and PLA signal, respectively. Integration times were optimized manually and then left constant for the whole chip image acquisition procedure. The images were analyzed using Matlab Image Processing Toolbox (Mathworks, Natick, MA). For cell segmentation, standard threshold and watershed algorithms were used.

## RESULTS

**Design of the Integrated Microfluidic Chip**—The microfluidic chip consists of three functional layers: two PDMS layers for the fluidic and control channel networks, and a glass substrate. The bottom glass layer provides a well-characterized surface for adherent cell cultures. The core elements of the fluidic layer are 128 separated cell culture chambers arranged in a 16 × 8 matrix. Each cell culture chamber has an area of 0.2 mm<sup>2</sup> and volume of about 10 nL. About 540 integrated valves in pushdown configuration control the fluid stream in the flow channel network. Fig. 1A shows an overview of the microfluidic chip design; the flow and control channel networks are filled with blue and red colored fluids, respectively. Fig. 1B illustrates the addressability of the cell culture compartments in the matrix format. Each row and column of the matrix can be addressed individually. With this two-dimensional approach, it is possible to multiplex two assay parameters, for example, the time intervals after chemical stimulation in column and primary Abs for the PLA in the row direction. The general matrix design also allows the variation of other assay parameters, for example, concentrations and/or different stimulation compounds. Cell cultures at each cross-point of the matrix encode for one combination of the variables.

The time resolution for a cell-stimulation experiment on chip is governed by the exchange time of a fluid in all connected microchambers in the row or column direction of the matrix. For determination of the time resolution of the PLA chip, we measured the flow rate within the chip with seeded fibroblast cells. At an applied flow pressure of 10 kPa, the volume flow was about  $1.0 \pm 0.1 \mu\text{L}/\text{min}$ . With the known total volumes of 120 and 200 nL per column and row, theoretical exchange rates of about 7 and 12 s are calculated, respectively. We

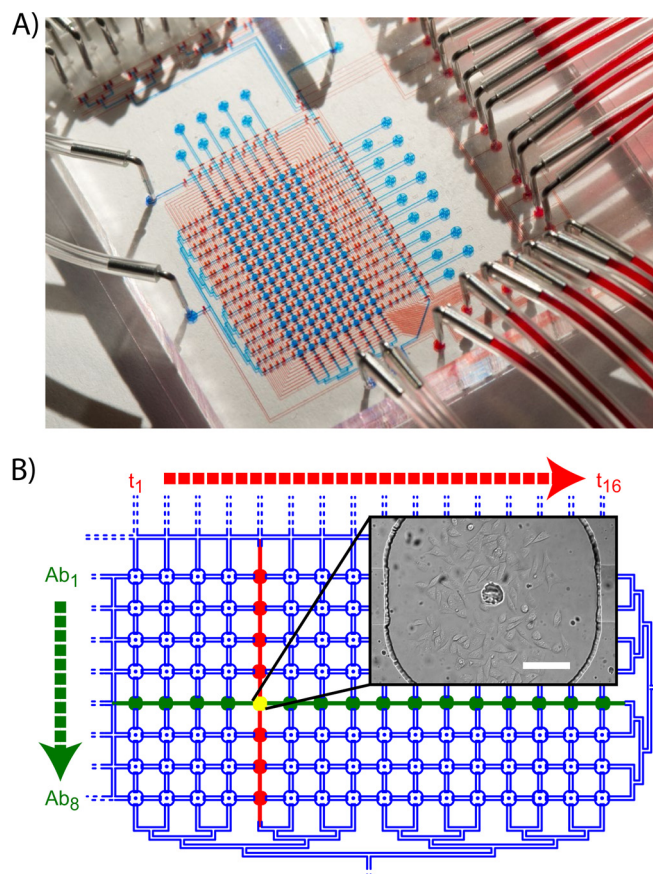


**Fig. 1. Large-scale integrated microfluidic chip.** A, image of the chip. Microchannels are filled with aqueous solution colored in red and blue for illustration of the control and flow channels, respectively. The whole device has an area of 40 mm × 45 mm. B, illustration of the matrix design for the arrangement of the cell culturing chambers. Each row and column of the matrix can be addressed individually, allowing the independent variation of two assay parameters (for example, 16 stimulation times and eight antibodies). Inset: exemplary cell culture chamber with cultivated NIH3T3 mouse embryonic fibroblasts. Scale bar = 100  $\mu\text{m}$ .

confirmed this value experimentally with alternating flush cycles of colored and clear buffer solutions. The highest achievable time resolution of cell-stimulation experiments on chip is twice the value of the exchange rate, because activation and fixation solution have to be flushed sequentially.

**Cell Culturing on Chip**—Homogeneous cell distributions of  $75 \pm 25$  fibroblast cells per culture chamber were obtained by introducing cell suspension in the column direction with a concentration of  $7 \times 10^6$  cells/ml. Micromechanical cell catching structures within the cell chambers were not required to hold the cells in the chambers. NIH3T3 and MEF cells attached within 10 min to the fibronectin-coated glass surface. Following feeding flush cycles with medium at 10 kPa removed only dead cells. In cases where the cell density in a cell culture chamber was too low, a second flush cycle with the cell suspension was applied. Cells attached to surfaces outside the matrix elements were removed with a short trypsin

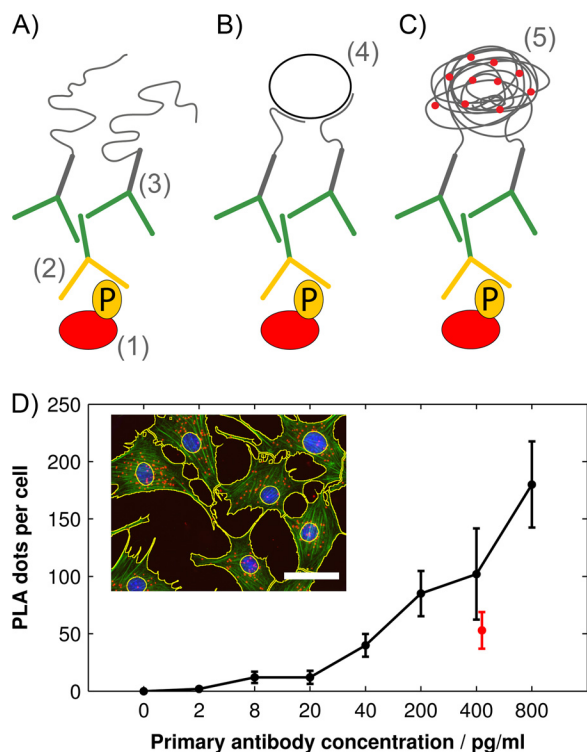


**FIG. 2. PLA on chip.** A–C, working principle of the integrated PLA. Primary antibody (2) and secondary antibody pair (3) bind to the target protein or phosphorylation sites (1) in the cell. Oligonucleotide labels of the secondary antibodies can be complemented with the help of a DNA connector (4) strand in cases where the two labels are in close proximity. The DNA connector is amplified via rolling circle amplification and detected with a fluorescence-labeled DNA probe molecule (5). During the PLA, the readout signal is transferred from protein to DNA level. D, on-chip PLA with varying anti-Akt primary antibody concentrations. The PLA was performed as depicted in panels A–C. PLA dots are counted on the single-cell level. The median value and the median absolute deviation of the PLA dots of all cells in one microfluidic cell chamber are plotted against the anti-Akt Ab concentration. The red data point at 400 pg/ml was obtained by performing an on-chip PLA experiment using two different, rather than one primary, anti-Akt antibodies under the same conditions. Inset: representative cell image obtained from a PLA experiment. PLA dots, cytoskeleton, and nuclei are counterstained with a probe molecule (red), phalloidin (green), and DAPI (blue). Cell segmentation lines obtained via standard image analysis are included (yellow). Image contrast was adjusted for printing. Scale bar = 50  $\mu\text{m}$ .

pulse. To maintain a viable fibroblast culture on chip, the medium in the microchambers was exchanged every 1.5 h. Reduction or prolongation of the medium flush cycles led to reduced cell viability. Under full medium conditions, the cells survived for at least 96 h, whereas under FBS starvation conditions they survived for only 24 h.

**Proximity Ligation Assay on Chip**—The PLA approach chosen in this study to detect protein phosphorylation and protein locations is summarized in Fig. 2A–C. Sequential operational steps of the PLA are divided into two blocks for implementation, that is, cell preparation and target detection. Fluids required for both blocks are integrated with the help of a fluid

multiplexer, which is a bifurcating channel network with inlet ports controlled by valves. The cell preparation block is a sequence of flow steps for the perfusion of cell fixation, permeabilization, and blocking reagents. Column elements of the matrix were separated from each other and addressed individually in order to avoid cross-contamination. Conditions for the single process steps are given in the “Experimental Procedures” section. The target detection block contains the perfusion and incubation of the primary and secondary Abs, ligation of the DNA labels, amplification via rolling circle amplification, and hybridization of the rolling circle amplification product to a detection probe for visualization. Full integration of both chemical blocks comprises about 2500 flow operations over 24 h. In contrast to classical off-chip PLA experiments, the cells are kept under defined environmental conditions, and dry-out effects leading to unspecific signals are avoided.

The general chip design also allowed the optimization of cell fixation and permeabilization parameters. For this, we exploited the two matrix dimensions to alternate the fixation time, paraformaldehyde concentration, and detergents and their concentrations by leaving the PLA conditions constant. The optimized parameters are given in the “Experimental Procedures” section and were derived based on the lowest variation of the PLA dot counts among repeats.

To demonstrate the successful implementation of the PLA, we measured the PLA dot counts per cell dependent on the primary antibody concentration in NIH3T3 cells. For this, we used a rabbit anti-Akt antibody specific for all Akt isoforms. The concentration of the anti-Akt antibody was altered in the row direction of the cell matrix, whereas the column dimension was kept constant and used for repeats. Fig. 2D shows the average PLA dot count per cell obtained for eight concentrations of the anti-Akt antibody. Single-cell resolution for the PLA dot count was obtained via image segmentation of the cells (see Fig. 2D, inset). In agreement with expectations, a linear relationship between the PLA events and the Akt antibody concentration was observed within the range of 20 to 800 pg/ml. We considered the optimal working concentration of an antibody as that at which the resulting PLA dot counts per cell were statistically reliable (>20 per cell) but not coalescent, so as to avoid saturation artifacts at higher antibody concentrations. We initially compared the dot counts obtained in PLA experiments with one and two different host-specific primary antibodies against Akt at a concentration of 400 pg/ml. The relative cell-to-cell variation in both PLA approaches was comparable (see red data point in Fig. 2D). Thereafter we used the PLA approach with a single primary Ab for all experiments, because matched primary Abs were not available for all targets.

**Phosphorylation Dynamics of the Akt Signaling Pathway**—The PLA chip was used to resolve the dynamics of signal transduction of the Akt pathway upon PDGF stimulation. PDGF regulates cell growth and division in various cell types

## PDGF (100 ng/ml) stimulation time variation

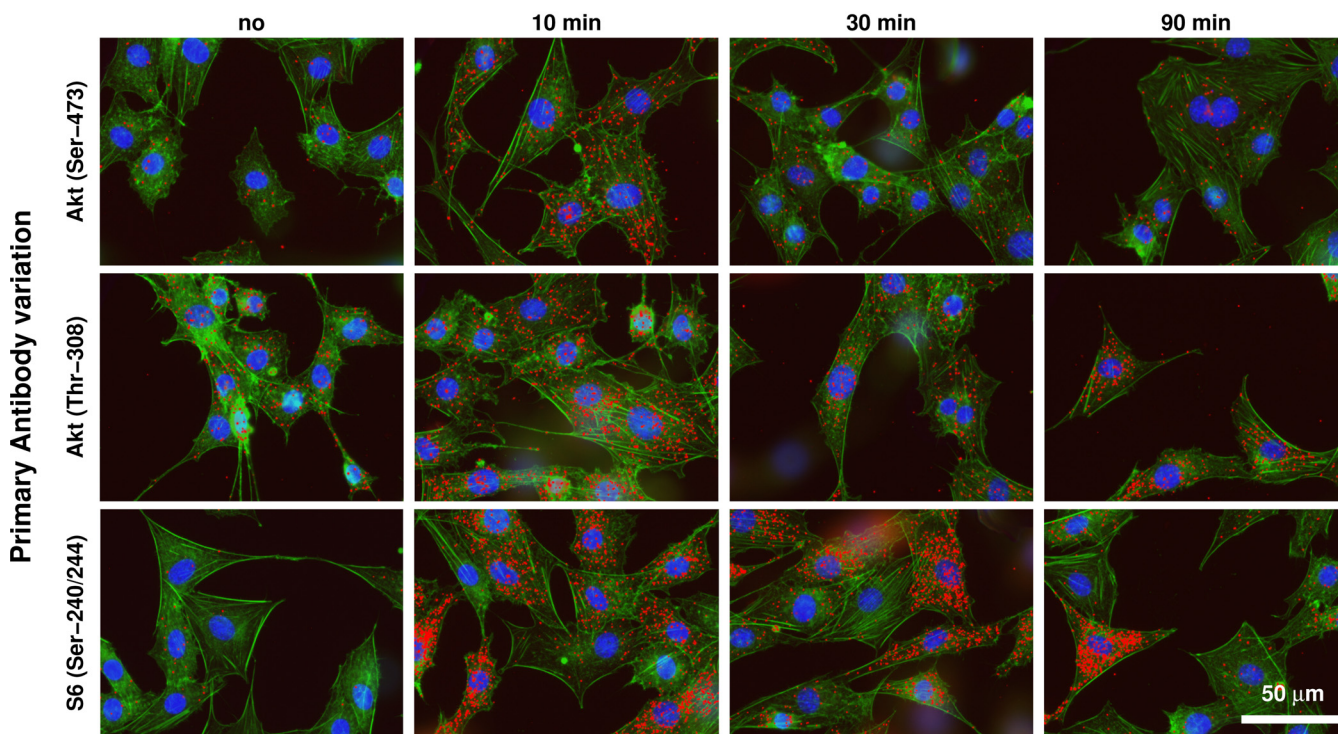
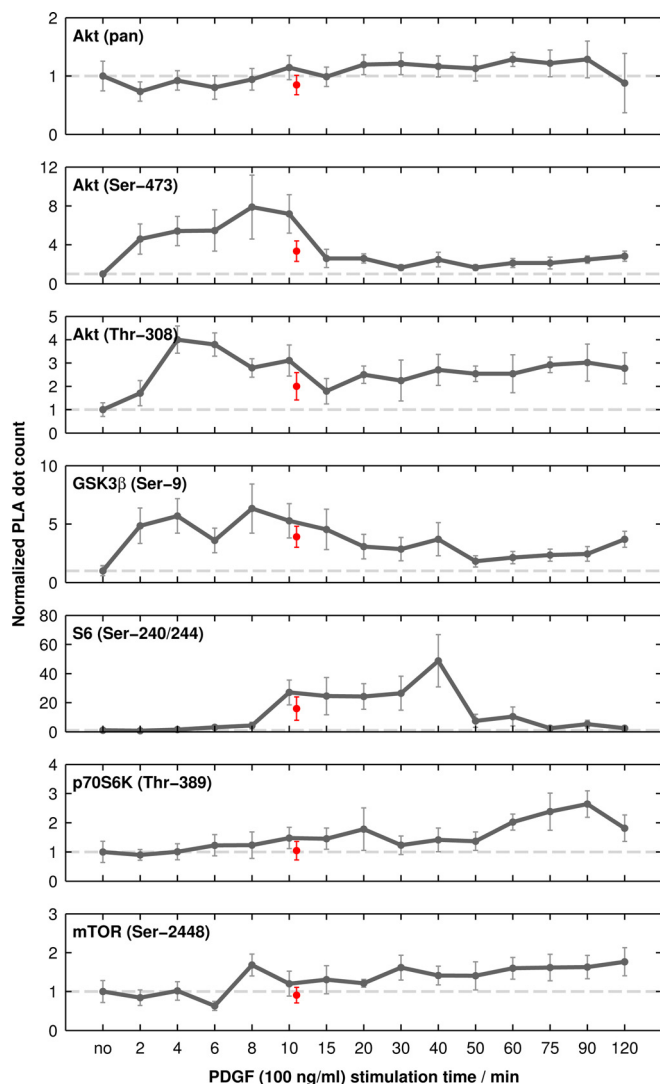


FIG. 3. Profiling of the Akt cell signaling pathway upon PDGF stimulation with the PLA. Subset of images of NIH3T3 cells upon PDGF stimulation on chip. The PLA dot counts per cell for the Akt Ser-473, Thr-308, and S6 Ser-240/244 antibody increased in response to 100 ng/ml PDGF stimulation. Quantitative analysis of the change in PLA dot count with PDGF stimulation time is presented in Fig. 4. PLA signals for both phosphorylation sites of Akt increased homogeneously in the ensemble of cells from one cell culture chamber. In contrast, the PLA signal corresponding to the phosphorylation site of S6 showed stochastic variation among cells from one condition. Image contrast was adjusted for printing using equal settings for all images. Scale bar = 50  $\mu\text{m}$ .

(14, 15). The signal transduction through the Akt pathway is described in detail elsewhere (16, 17). In short, the stimulation of mouse fibroblast cells with PDGF leads to phosphorylation of the PDGF receptor and the production of PIP3 through PIP3 kinase. Akt is recruited to the membrane upon binding to PIP3 and is phosphorylated by PDK1 (18) and the rapamycin insensitive mTOR complex 2 (mTORC2) at its residues Thr-308 and Ser-473, respectively (19). Activated Akt propagates the signal downward by phosphorylating GSK-3 $\beta$  (Ser-9) (20) and FoxO3a (Thr-32 and Ser-253) (21). In response to the phosphorylation, FoxO3a changes its cellular position from nucleus to cytoplasm. In parallel, PDGF also activates the rapamycin-sensitive mTOR complex 1 (mTORC1). The mTORC1 activates protein synthesis through phosphorylation of the p70S6 kinase (Thr-389), which in turn phosphorylates the 40S ribosomal S6 protein (22). The phosphorylation states of mTORC1, GSK-3 $\beta$ , and S6 and the position of FoxO3a are reporters of the cellular metabolic, transcriptional, and translational state of the cell. Therefore, monitoring the phosphorylation states of the two Akt residues, GSK-3 $\beta$ , mTOR, p70S6K, and S6 or the cellular location of FoxO3a in parallel and over time gives a detailed view of signal transduction within the Akt pathway upon PDGF stimulation.

For cell stimulation experiments, NIH3T3 cells were starved for 14 h on chip and stimulated with PDGF at a concentration of 100 ng/ml. Fourteen columns of the chip were allocated to stimulation time intervals between 2 and 120 min. In the two remaining columns of the chip, control experiments were performed involving (i) no PDGF stimulation and (ii) inhibition of the phosphatidylinositol(3,4,5)-trisphosphate (PIP3) kinase with LY294002 before PDGF stimulation. Primary antibodies used in the PLA reaction were multiplexed in the row direction of the cell culture matrix. Fig. 3 shows an exemplary subset of images obtained from the stimulation experiment for the phosphorylation targets Akt Ser-473, Thr-308, and S6 Ser-240/244. Fig. 4 shows the corresponding quantitative analysis of the PLA dot counts per cell for all targets measured dependent on the PDGF stimulation time. The PLA signals were normalized to the control experiment without PDGF stimulation. For Akt, a constant PLA dot count was observed within the 2 h of PDGF stimulation, which is in agreement with the expectation. Further, this result demonstrates the homogeneity of the automated PLA assay on chip over all elements of the cell culture matrix.

In contrast, PLA dot counts for the Akt Ser-473 and Thr-308 phosphorylation sites increased strongly within the first 10



**FIG. 4. Quantitative PLA analysis of phosphorylation signals within the Akt pathway upon PDGF stimulation.** Normalized median PLA dot counts per cell for total Akt, Akt Ser-473, Akt Thr-308, GSK-3 $\beta$  Ser-9, S6 Ser-240/244, p70S6K Thr-389, and mTOR Ser-2448 versus PDGF stimulation time. PLA dot counts are normalized to the no-stimulation conditions. Red data points in all plots denote the control experiment with the PIP3 kinase inhibitor LY294002. For this, cells were incubated with LY294002 for 30 min before stimulation with PDGF. All experiments were performed on one microfluidic chip with NIH3T3 cells.

min after PDGF stimulation. The increase of the PLA dot count for the phosphorylation of the Ser-9 residue of GSK-3 $\beta$  followed the same kinetics as the Akt phosphorylation sites, whereas PLA signals indicative of the phosphorylation site of S6 were shifted by 8 to 10 min after the PDGF stimulation. A sharp return of the PLA signal to basal level was observed for Akt Ser-473 and S6, whereas GSK-3 $\beta$  and Akt Thr-308 phosphorylation showed a slower decay. For the phosphorylation sites of p70S6K and mTOR, a slight but steady increase of the PLA signal was observed during the 2h time interval. PLA results with the PIP3 kinase inhibitor LY294002 are shown in

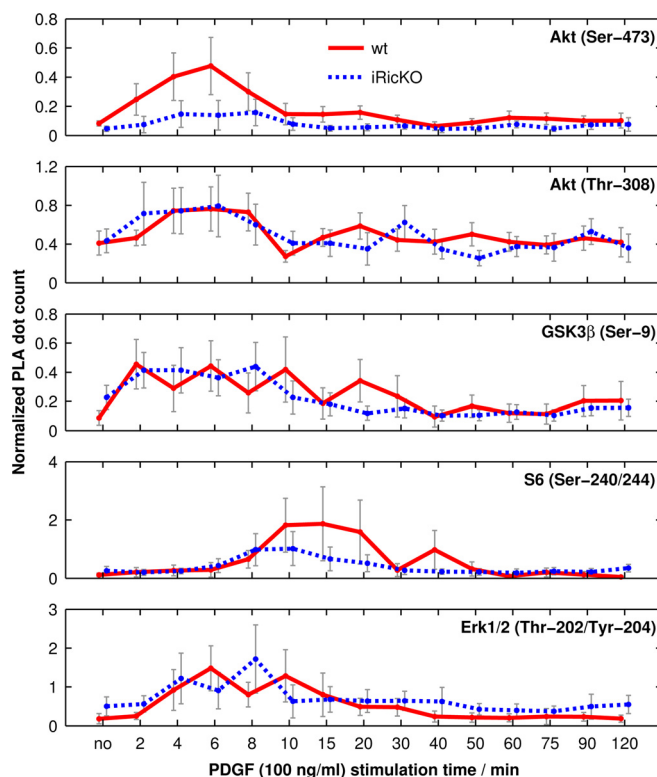


**FIG. 5. Quantitative PLA analysis of phosphorylation signals within rictor deficient and wild-type MEF cells upon PDGF stimulation.** Normalized median PLA dot counts per cell for Akt Ser-473, Akt Thr-308, GSK-3 $\beta$  Ser-9, S6 Ser-240/244, and Erk1/2 Thr-202/Tyr-204 versus PDGF stimulation time in iRicoKO (blue dotted line) and wild-type (red solid line) MEF cells. For comparison, all PLA dot counts were normalized to the median PLA signal of total Akt, which was constant over the time frame of the stimulation experiment.

Fig. 4 as red dots at the time point of 10 min. Inhibition of the PIP3 kinase prior to PDGF stimulation led to a reduction by at least of a factor of 2 of the PLA dot counts per cell for Akt Ser-473, Akt Thr-308, and S6 in comparison to non-inhibited cells. Minor PLA signal reduction was observed for the GSK-3 $\beta$ , mTOR, and p70S6K phosphorylation.

To confirm our PLA results, we repeated the PDGF stimulation experiment with two MEF cell lines, a wild type and a rictor inducible deficient MEF cell line (iRicoKO). Upon growth factor or serum stimulation, mTOR complexed with rictor (mTORC2) phosphorylates Akt at residue Ser-473. For iRicoKO cells, it has been demonstrated that Akt Ser-473 phosphorylation is largely reduced in comparison with the wild-type MEF cell line. The knockdown of rictor within iRicoKO cells after 72 h of tamoxifen treatment was confirmed with a Western blot analysis (data omitted). Fig. 5 shows the PLA dot counts per cell within the two MEF cell lines for the Akt Ser-473, Thr-308, GSK-3 $\beta$ , S6, and Erk1/2 phosphorylation sites upon PDGF stimulation. We found that the amplitude of the PLA signals for the Akt Ser-473 and S6 phosphorylation was diminished by a factor of 3 and 2, respectively within iRicoKO relative to wild-type cells upon PDGF stimulation. The kinetics and am-

plitudes of the PLA signals for Akt Thr-308 and GSK-3 $\beta$  phosphorylation were equal in both cell lines. Additionally, we included the phosphorylation signal of Erk1/2 Thr-202/Tyr-204 kinase within the experimental series as a control. Erk1/2 protein is member of the MAPK pathway, and its phosphorylation in response to PDGF stimulation is independent of rictor. Fig. 5 shows the unchanged PLA signals for the Erk1/2 phosphorylation in iRicoKO and wild-type cells upon PDGF stimulation.

**Translocation Dynamics within the Akt Signaling Pathway**—In the last step, we analyzed the dynamic changes of the subcellular position of FoxO3a upon PDGF stimulation. FoxO3a belongs to the forkhead family of transcription factors and is directly phosphorylated by Akt inside the nucleus (23). Gene transcription of FoxO3a targets is inhibited through translocation of FoxO3a out of the nucleus. To detect the translocation of FoxO3a, we used an antibody against the N-terminal end of FoxO3a rather than an antibody for its phosphorylation site. This ensured detection of the protein in its phosphorylated and dephosphorylated states. Fig. 6A–D show micrographs of NIH3T3 cells with PLA signals before and after representative time intervals of PDGF stimulation. The same experiments were additionally included within the chip runs with wild-type and iRicoKO MEF cells. Fig. 6E summarizes the fractional changes of PLA dot counts per nucleus to PLA dot counts per cell with PDGF stimulation time for the NIH3T3 and two MEF cell lines. Within the NIH3T3 and MEF wild-type cells, the fraction of PLA dots located in the nucleus decreased by 30% within the first 6 min and then recovered to basal level after 30 to 50 min of PDGF stimulation. Notably, the kinetics of FoxO3a translocation measured by the PLA correlates with the PLA dot count kinetics of the Akt phosphorylation. A PLA translocation signal from nucleus to cytoplasm for FoxO3a upon PDGF stimulation could not be detected within iRicoKO cells. In fact, the absolute number of PLA dots for FoxO3a in iRicoKO cells was clearly decreased by a factor of 3 to about 20 PLA dots per cell compared with the two wild-type fibroblast cells.

#### DISCUSSION

Quantitative protein analytical technologies used in higher-throughput work are required to leverage theoretical and systems cell signaling research. Here we integrated 128 cell cultures together with the proximity ligation assay in a high parallel fashion on a microfluidic chip. We used the technological advantages of integrated microfluidic flow logics to obtain temporal and spatial resolution of protein phosphorylation and translocation changes during growth factor activation of the Akt signaling pathway in multiple fibroblast cell lines.

Miniaturization of mammalian cell cultures on microfluidic chips has been accomplished for various applications (24, 25). The microfluidic platform engineered here allowed the maintenance of cell cultures for at least 96 h on the substrate,

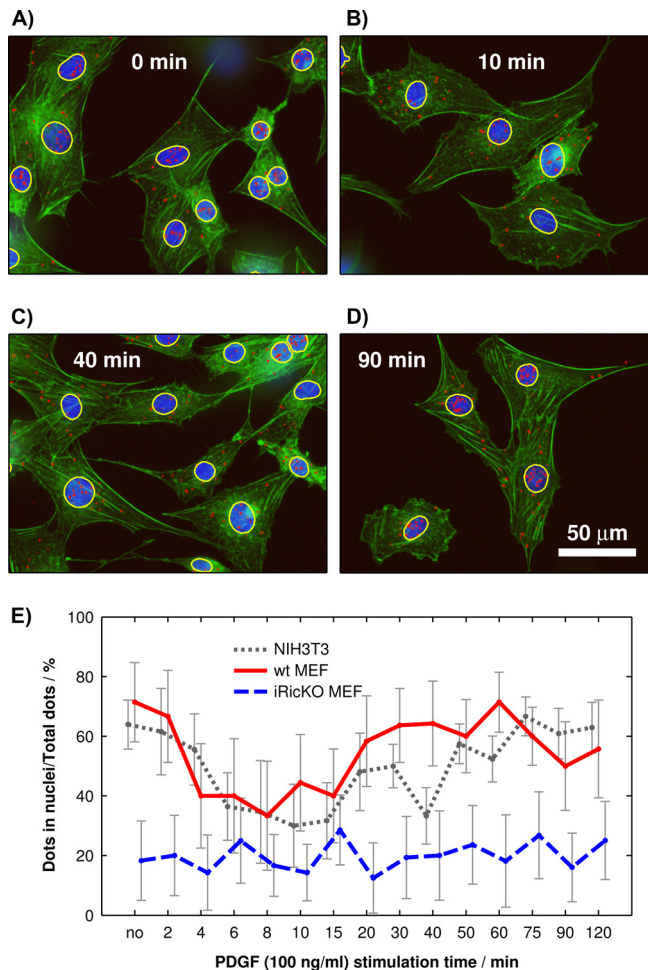


**Fig. 6. Cellular translocation of FoxO3a upon PDGF stimulation.** A–D, fluorescence images with PLA signals corresponding to FoxO3a in nonstimulated cells and after 10, 40, and 90 min of 100 ng/ml PDGF stimulation in NIH3T3 cells. The ratio of PLA dots within the nucleus and cytoplasm changed upon PDGF stimulation. The image contrast was adjusted for plotting using equal settings for all images. Scale bar = 50  $\mu$ m. Segmentation lines for the nuclei are depicted in yellow. E, quantitative cellular position analysis of PLA dots corresponding to FoxO3a in NIH3T3 (black dotted line), iRicoKO (blue dashed line), and wild-type (red solid line) MEF cells. The plot shows the changes in the ratio of PLA dots in the nuclei to PLA dots in the whole cell in response to PDGF stimulation time. Within MEF wild-type and NIH3T3 cells, the PLA signal of FoxO3a in the nucleus decreased by 30% after 6 min and recovered after about 30 to 50 min. PLA signals of FoxO3a in the iRicoKO MEF cells showed no change in position upon PDGF stimulation.

including adherence, starvation, and/or synchronization phases. Automated cell feeding on chip obviated nutrient depletion of cells in microchambers. Further, the control over the cell microenvironment could be used to precisely stimulate cells in time intervals of minutes. A higher time resolution for cell signaling studies on chip is possible, but an estimated lower limit due to technical constraints is 2 to 3 s. In contrast to manual cell culturing workflows, the microfluidic chip can enable complex stimulation patterns with different pulse

lengths, amplitudes, and repetitions in future experiments. Next to the cell culture platform, we integrated in a multiplexed fashion the PLA technology on the chip. Advantages of PLA including single-molecule detection, high sensitivity, and cellular position information are thus accessible for higher-throughput science. In contrast to classical PLA experiments performed on glass slides, the chip provides the constant conditions required for data comparison. Our consistent PLA dot counts on the same targets in three different fibroblast cell lines and tens of different conditions demonstrated the repeatability of the chip PLA. Accompanying the miniaturization of the PLA technology was a reduced Ab consumption by 2 orders of magnitude relative to off-chip assay conditions.

Akt is a pivotal protein kinase with regulative function in the cell metabolism, growth, and survival network. Defects in the Akt signaling cascade are found in various cancer cells (26). The activity of Akt is regulated via phosphorylation of its residues Ser-473 and Thr-308, and full kinase activation requires the phosphorylation of both residues (27). Activation of the Akt signaling pathway can be initiated by various growth factors including PDGF, IGF-1, and insulin. The first step of the PDGF signaling event is the autophosphorylation of the PDGF receptor upon growth factor binding (28). PDGF receptor phosphorylation in dose response to PDGF has been determined with PLA on human foreskin fibroblasts with a resulting  $EC_{50}$  of 30 to 40 ng/ml (29). Here, we used a PDGF concentration at saturation conditions (100 ng/ml) to activate the PDGF receptor. PLA targets within the Akt signaling pathway were chosen as representative of the signal transduction and change of the cellular state upon growth factor stimulation.

PLA results revealed phosphorylation and dephosphorylation of Akt Ser-473 and Thr-308 within NIH3T3 and wild-type MEF cells after 2 and 8 to 10 min upon PDGF stimulation, respectively. The phosphorylation response times for both Akt phosphorylation sites are in agreement with values measured previously with ELISA and fluorescence assay techniques (4, 11, 30), whereas dephosphorylation response times were shorter than reported values of 15 to 120 min. Lower PDGF concentrations, longer cell-starvation times, and different cell lines used within reported experiments can explain the differences.

Notably, the phosphorylation response time of GSK-3 $\beta$  and the nucleus-to-cytoplasm translocation time of FoxO3a followed the same phosphorylation response times of the two Akt residues. This is expected because GSK-3 $\beta$  and FoxO3a are direct targets of Akt (20, 23). We also evaluated all other PLA signals for position changes from nucleus and cytoplasm or vice versa after PDGF stimulation but could not find any significant changes.

As a second signaling branch within the Akt signaling cascade, we monitored the phosphorylation of mTOR, p70S6K, and S6 proteins. Phosphorylation of mTOR at Ser-2448 is commonly used as a biomarker for the activation state of the

PI-3 kinase pathway (31). The activity of mTOR kinase itself is dependent on multiple phosphorylation events and protein interaction partners, and therefore the phosphorylation state of the Ser-2448 residue is only an indicator of the kinase activity state. Within mammalian cells, mTOR forms two distinct multiprotein complexes, the rapamycin-sensitive and -insensitive mTORC1 and mTORC2 complexes, respectively. The mTORC1 complex is known to phosphorylate p70S6K at residue Thr-389 in response to growth factor stimulation (32), and in reverse p70S6K phosphorylates mTOR at the residue Ser-2448 (31). Activated p70S6 kinase transmits the growth factor signal to the S6 protein via phosphorylation of the Ser-240/244 residues (22). S6 is a regulatory component of the 40S ribosome, and the phosphorylation of S6 assists the initiation of ribosomal protein synthesis.

The phosphorylation response times of mTOR and p70S6K measured here are clearly slower than the phosphorylation kinetics of the two Akt residues within NIH3T3 cells. The PLA signal for the Ser-2448 and Thr-389 phosphorylation of mTOR and p70S6K increased over the 120 min of PDGF stimulation linearly by a factor of 2. Both phosphorylation sites are mutually dependent because of the direct interaction between the two kinases, and thus a similar response time was observed before (33). The PLA results for the downward signal of the S6 phosphorylation at residue Ser-240/244, however, exhibit a sharp and defined on-and-off response between 8 and 20 min of PDGF stimulation. Notably, in the PLA experiments on the S6 protein we observed strong statistical variation from cell to cell in one chamber under the same conditions. The S6 signal variation between cells is reflected in the larger error bars of the PLA signal for activated S6 protein in NIH3T3 and MEF wild-type cells (see Figs. 4 and 5). The corresponding micrograph is shown in Fig. 3 (bottom, 30 min), in which it is shown that about half of the cells exhibited a strong PLA signal for the S6 phosphorylation and the other half did not. This finding argues for a threshold behavior and was observed only for phosphorylation and dephosphorylation of S6.

In general, antibody-based *in situ* detection systems suffer from false positive signals due to unspecific binding. To exclude false positive PLA signals and validate the quantitative PLA readout, we performed (i) chemical inhibitor and (ii) biological control experiments. With the help of the PIP3 kinase inhibitor LY294002, the PDGF signaling cascade was interrupted upstream of Akt. NIH3T3 cells incubated with LY294002 before PDGF stimulation exhibited a reduced PLA dot count for the phosphorylation sites of the two Akt residues, GSK-3 $\beta$  and S6, compared with noninhibited cells. MEF cells deficient for rictor were used for biological control of the PLA experiments. Rictor is the scaffold protein within the mTORC2, which catalyzes the phosphorylation of Akt Ser-473 (19). Knockdown of rictor leads to reduced Akt phosphorylation upon serum or growth factor stimulation (19). Indeed, the PLA dot count for the Akt Ser-473 phosphorylation was re-

duced by a factor of 3 within iRicKO relative to wild-type MEF cells. The reduced fraction of fully activated Akt in the iRicKO cells upon PDGF stimulation, however, resulted not in a reduction of the GSK-3 $\beta$  phosphorylation but in a loss of the translocation signal of FoxO3a. This finding is in agreement with Akt stimulation studies with the iRicKO cell line (34). In the case of the translocation signal of FoxO3a in the iRicKO cells, the PLA dot count indicated a down-regulation of the total amount of FoxO3a relative to the wild-type cells. Thus, the loss of translocation signal for FoxO3a in iRicKO cells could be caused by a low number of PLA signals.

PLA results of the iRicKO cells also showed reduced S6 phosphorylation. Previous Western blot experiments with an iRicKO cell line did not reveal any changes of S6 phosphorylation upon PDGF stimulation (35). The stochastic behavior of the PLA signal and the accompanied increased of cell-to-cell variation could account for the reduction of the S6 phosphorylation measured for iRicKO cells. Nevertheless, the single-cell resolution of the PLA assay technology applied in a systematic approach can help to unravel the difference in signal transduction between cell populations.

In summary, we have demonstrated that the integrated advances of PLA, including single-molecule resolution and cellular position analysis, allowed high-content screening of the Akt cell signaling pathway. It can be expected that minor engineering steps will lead to an increase in throughput by a factor of 4 in the next chip generation. Further, rearrangements of the chip logics and process steps are currently being investigated to decrease the run time of PLA to hours. The general design of the microfluidic chip is not limited to the detection of protein phosphorylation events and is also applicable for protein interaction or other post-translational modification measurements.

\* This study was supported by the German Excellence Initiative (BIOSS-Project C7) and by the German Research Foundation (Emmy-Noether Grant ME3823/1-1).

§§ To whom correspondence should be addressed: E-mail: Matthias.meier@imtek.de.

## REFERENCES

- Muzzey, D., and van Oudenaarden, A. (2009) Quantitative time-lapse fluorescence microscopy in single cells. *Annu. Rev. Cell Dev. Biol.* **25**, 301–327
- Simpson, J. C., Joggerst, B., Laketa, V., Verissimo, F., Cetin, C., Erfle, H., Bexiga, M. G., Singan, V. R., Hériché, J. K., Neumann, B., Mateos, A., Blake, J., Bechtel, S., Benes, V., Wiemann, S., Ellenberg, J., and Pepperkok, R. (2012) Genome-wide RNAi screening identifies human proteins with a regulatory function in the early secretory pathway. *Nat. Cell Biol.* **14**, 764–774
- Ma, H., Gibson, E. A., Dittmer, P. J., Jimenez, R., and Palmer, A. E. (2012) High-throughput examination of fluorescence resonance energy transfer-detected metal-ion response in mammalian cells. *J. Am. Chem. Soc.* **134**, 2488–2491
- Kunkel, M. T., Ni, Q., Tsien, R. Y., Zhang, J., and Newton, A. C. (2004) Spatio-temporal dynamics of protein kinase B/Akt signaling revealed by a genetically encoded fluorescent reporter. *J. Biol. Chem.* **280**, 5581–5587
- Herman, B. *Fluorescence Microscopy*, 2nd ed., Bios Scientific Publishers, Oxford, UK, 1998
- Fredriksson, S., Gullberg, M., Jarvius, J., Olsson, C., Pietras, K., Gústafsdóttir, S. M., Ostman, A., and Landegren U. (2002) Protein detection using proximity-dependent DNA ligation assays. *Nat. Biotechnol.* **20**, 473–477
- Söderberg, O., Gullberg, M., Jarvius, M., Ridderstråle, K., Leuchowius, K. J., Jarvius, J., Wester, K., Hydbring, P., Bahram, F., Larsson, L. G., and Landegren, U. (2006) Direct observation of individual endogenous protein complexes in situ by proximity ligation. *Nat. Methods* **3**, 995–1000
- Allalou, A., and Wählby, C. (2009) BlobFinder, a tool for fluorescence microscopy image cytometry. *Comput. Methods Programs Biom.* **94**, 58–65
- McDonald, J., and Whitesides, G. (2002) Poly(dimethylsiloxane) as a material for fabricating microfluidic devices. *Accounts Chem. Res.* **35**, 491–499
- Tay, S., Hughey, J. J., Lee, T. K., Lipniacki, T., Quake, S. R., and Covert, M. W. (2010) Single-cell NF- $\kappa$ B dynamics reveal digital activation and analogue information processing. *Nature* **466**, 267–271
- Cheong, R., Wang, C. J., and Levchenko, A. (2009) High content cell screening in a microfluidic device. *Mol. Cell. Proteomics* **8**, 433–442
- Hughes, A. J., and Herr, A. E. (2012) Microfluidic Western blotting. *Proc. Natl. Acad. Sci. U.S.A.* **109**, 21450–21455
- Meier, M., Sit, R., Pan, W., and Quake, S. R. (2012) High-performance binary protein interaction screening in a microfluidic format. *Anal. Chem.* **21**, 9572–9578
- Hannink, M., and Donoghue, D. J. (1989) Structure and function of platelet-derived growth factor (PDGF) and related proteins. *Biochim. Biophys. Acta* **989**, 1–10
- Kim, H. R., Upadhyay, S., Li, G., Palmer, K. C., and Deuel, T. F. (1995) Platelet-derived growth factor induces apoptosis in growth-arrested murine fibroblasts. *Proc. Natl. Acad. Sci. U.S.A.* **92**, 9500–9504
- Bozulic, L., and Hemmings, B. A. (2009) PI3K on PKB: regulation of PKB activity by phosphorylation. *Curr. Opin. Cell Biol.* **21**, 256–261
- Bhaskar, P. T., and Hay, N. (2007) The Two TORCs and Akt. *Dev. Cell* **12**, 487–502
- Walker, K. S., Deak, M., Paterson, A., Hudson, K., Cohen, P., and Alessi, K. S. (1998) Activation of protein kinase B beta and gamma isoforms by insulin in vivo and by 3-phosphoinositide-dependent protein kinase-1 in vitro: comparison with protein kinase B alpha. *Biochem. J.* **331**, 299–308
- Sarbassov, D. D., Guertin, D. A., Ali, S. M., and Sabatini, D. M. (2005) Phosphorylation and regulation of Akt/PKB by the rictor-mTOR complex. *Science* **307**, 1098–1101
- Cross, D. A., Alessi, D. R., Cohen, P., Andjelkovich, M., and Hemmings, B. A. (1995) Inhibition of glycogen synthase kinase-3 by insulin mediated by protein kinase B. *Nature* **378**, 785–789
- Brunet, A., Bonni, A., Zigmond, M. J., Lin, M. Z., Juo, P., Hu, L. S., Anderson, M. J., Arden, K. C., Blenis, J., and Greenberg, M. E. (1999) Akt promotes cell survival by phosphorylating and inhibiting a forkhead transcription factor. *Cell* **96**, 857–868
- Krieg, J., Hofsteenge, J., and Thomas, G. (1988) Identification of the 40 S ribosomal protein S6 phosphorylation sites induced by cycloheximide. *J. Biol. Chem.* **263**, 11473–11477
- Biggs, W. H., III, Meisenhelder, J., Hunter, T., Cavenee, W. K., and Arden, K. C. (1999) Protein kinase B/Akt-mediated phosphorylation promotes nuclear exclusion of the winged helix transcription factor FKHR1. *Proc. Natl. Acad. Sci. U.S.A.* **96**, 7421–7426
- Lecault, V., VanInsberghe, M., Sekulovic, S., Knapp, D. J. H. F., Wohrer, S., Bowden, W., Viel, F., McLaughlin, T., Jarandehi, A., Miller, M., Falconnet, D., White, A. K., Kent, D. G., Copley, M. R., Taghipour, F., Eaves, C. J., Humphries, R. K., Piret, J. M. and Hansen, C. L. (2011) High-throughput analysis of single hematopoietic stem cell proliferation in microfluidic cell culture arrays. *Nat. Methods* **8**, 581–586
- Gómez-Sjöberg, R., Leyrat, A., Pirone, D., Chen, C., and Quake, R. S. (2007) Versatile, fully automated, microfluidic cell culture system. *Anal. Chem.* **79**, 8557–8563
- Manning, B. D., and Cantley, L. C. (2007) AKT/PKB signaling: navigating downstream. *Cell* **129**, 1261–1274
- Alessi, D. R., Andjelkovic, M., Caudwell, B., Cron, P., Morrice, N., Cohen, P., and Hemmings, D. R. (1996) Mechanism of activation of protein kinase B by insulin and IGF-1. *EMBO J.* **15**, 6541–6551
- Kelly, J. D., Haldeman, B. A., Grant, F. J., Murray, M. J., Seifert, R. A., Bowen-Pope, D. F., Cooper, J. A., and Kazlauskas A. (1991) Platelet-derived growth factor (PDGF) stimulates PDGF receptor subunit

- dimerization and intersubunit trans-phosphorylation. *J. Biol. Chem.* **266**, 8987–8992
29. Jarvius, M., Paulsson, J., Weibrecht, I., Leuchowius, K. J., Andersson, A. C., Wählby, C., Gullberg, M., Botling, J., Sjöblom, T., Markova, B., Ostman, A., Landegren, U., and Söderberg, O. (2007) In situ detection of phosphorylated platelet-derived growth factor receptor beta using a generalized proximity ligation method. *Mol. Cell. Proteomics* **6**, 1500–1509
30. Park, C. S., Schneider, I. C., and Haugh, J. M. (2003) Kinetic analysis of platelet-derived growth factor receptor/phosphoinositide 3-kinase/Akt signaling in fibroblasts. *J. Biol. Chem.* **278**, 37064–37072
31. Chiang, G. G., and Abraham, R. T. (2005) Phosphorylation of mammalian target of rapamycin (mTOR) at Ser-2448 is mediated by p70S6 kinase. *J. Biol. Chem.* **280**, 25485–25490
32. Holz, M. K. (2005) Identification of S6 kinase 1 as a novel mammalian target of rapamycin (mTOR)-phosphorylating kinase. *J. Biol. Chem.* **280**, 26089–26093
33. Dalle Pezze, P., Sonntag, A. G., Thien, A., Prentzell, M. T., Godel, M., Fischer, S., Neumann-Haefelin, E., Huber, T. B., Baumeister, R., Shanley, D. P., and Thedieck, K. (2012) A dynamic network model of mTOR signaling reveals TSC-independent mTORC2 regulation. *Sci. Signal.* **5**, ra25
34. Cybulski, N., Zinzalla, V., and Hall, M. N. (2012) Inducible raptor and rictor knockout mouse embryonic fibroblasts. *Methods Mol. Biol.* **821**, 267–278
35. Razmara, M., and Heldin, C. H. (2013) Platelet-derived growth factor-induced Akt phosphorylation requires mTOR/Rictor and phospholipase C- $\gamma$ 1, whereas S6 phosphorylation depends on mTOR/Raptor and phospholipase D. *Cell Commun. Signal.* **11**, 1–12
36. Unger, M. A., Chou, H. P., Thorsen, T., Scherer, A., and Quake, S. R. (2000) Monolithic microfabricated valves and pumps by multilayer soft lithography. *Science* **288**, 113–116